The Astrophysical Journal, 901:52 (10pp), 2020 September 20 https://doi.org/10.3847/1538-4357/abad39

A Modified Algorithm and Open-source Computational Package for the Determination of Infrared Optical Constants Relevant to Astrophysics

Perry A. Gerakines and Reggie L. Hudson
Astrochemistry Laboratory, NASA Goddard Space Flight Center, Greenbelt, MD 20771 USA; perry.a.gerakines@nasa.gov
Received 2020 June 2; revised 2020 August 4; accepted 2020 August 5; published 2020 September 21

Abstract

Infrared (IR) telescopes, such as Spitzer and SOFIA, have revealed a rich variety of chemical species trapped in interstellar ices. The most fundamental parameters to be derived from observed IR spectra are the identity and abundance of each component. Several compounds have been conclusively or tentatively identified, but the band strengths and optical constants needed to derive accurate abundances for many of these are poorly constrained. We have developed a modified approach to the extraction of the real and imaginary parts of the refractive index (optical constants) of a thin film from a single transmission spectrum measured in the IR spectral range. Our algorithm is similar to those implemented by previous authors, with some major changes that yield results for strong absorptions where previous approaches fail: (1) an adaptive *k*-correction step size, (2) the use of a root-finding algorithm to obtain a more accurate *k*-correction at each iteration, and (3) a *k*-correction step that prevents non-physical results such as negative *n*-values that prevent convergence in the calculation algorithm. The algorithm is presented and described, with examples to show agreement with some existing results and improvements upon others. New optical-constants calculations for CH_3OH, CO_2, N_2O, and CH_4 are presented, and potential implications for the modeling of interstellar and planetary ice data from space telescopes are discussed. With the objective of being open-source and transparent, the full source code in the free Python programming language is made available along with the compiled version and the laboratory data used to produce the results shown.

Unified Astronomy Thesaurus concepts: Molecular spectroscopy (2095); Astrochemistry (75); Laboratory astrophysics (2004)

1. Introduction

For any given material, the so-called optical "constants" $n(\tilde{\nu})$ and $k(\tilde{\nu})$ are the set of real and imaginary parts, respectively, of its complex refractive index $m(\tilde{\nu}) = n(\tilde{\nu}) - ik(\tilde{\nu})$.[1] In astronomy-related applications, a library of optical constants representing different materials is used to model the scattering of light from planetary surfaces, protoplanetary disks, and reflection nebulae, or to model the transmission and extinction of light as it passes through an interstellar cloud. Accurate laboratory determinations of $n(\tilde{\nu})$ and $k(\tilde{\nu})$ are required to reproduce the observed spectra and infer the composition and other physical properties of matter in these space environments.

There are a range of experimental methods for determining the values of n and k from films of solid materials, many of which are discussed by Heavens (1955) and involve knowledge of both the reflected and transmitted light over a wide spectral range. However, most laboratories are limited to measurements of either the transmittance or the reflectance. Methods for extracting optical constants from a single infrared (IR) transmittance spectrum of a film ($\lambda > 0.8\,\mu$m, $\tilde{\nu} < 12{,}500\,\mathrm{cm}^{-1}$) have existed for decades (e.g., Bergren et al. 1978), and one of the earliest examples in the laboratory astrophysics literature is a study by Hagen et al. (1981) on the optical constants of crystalline H_2O, followed later by, for example, Hudgins et al. (1993), Poteet et al. (2013), and Rocha & Pilling (2014).

In summary, the transmittance of light at wavenumber $\tilde{\nu}$ (in cm^{-1}) through a series of parallel layers can be expressed by a relatively simple analytical formula for a small number of layers and for an incidence angle of 0° (normal incidence). For an ice layer of thickness h, with refractive index $m = n - ik$, on a much thicker (essentially infinite) substrate in a vacuum, the transmittance of the ice can be written

$$T(n, k) = e^{-4\pi hk\tilde{\nu}} \left| \frac{t_{01}t_{12}}{1 + r_{01}r_{12}e^{-4i\pi hm\tilde{\nu}}} \right|^2 \frac{1}{|t_{02}|^2}, \qquad (1)$$

where t_{ij} and r_{ij} are the wavenumber-dependent, complex Fresnel coefficients for transmission and reflection at the interface from medium i into medium j:

$$t_{ij} = \frac{2m_i}{m_i + m_j} \qquad r_{ij} = \frac{m_i - m_j}{m_i + m_j}, \qquad (2)$$

where in Equation (1), the subscript "0" stands for vacuum, "1" for the ice layer, and "2" for the substrate. See Heavens (1955) for a derivation of the equations for these quantities, which are functions of the optical constants of the ice and of the substrate. Note that the second term in Equation (1) contains effects of both the sample and the substrate, and the transmittance spectrum of the bare substrate is removed by the division of the last term. It is also worth pointing out that while the resulting $T(n, k)$ spectrum is real-valued everywhere, its calculation involves complex arithmetic that may make it difficult to implement in certain commercial software applications. A

[1] Known as the "Nebraska convention," this definition of m was adopted as the standard in ellipsometry by Muller (1969) at the second international conference on ellipsometry at the University of Nebraska. The sign of the imaginary part of $m(\tilde{\nu})$ is a convention originating from the choice of sign in the exponential time dependence of the electromagnetic wave. This choice has no effect on the values of n or k nor on their usage. See the discussion by Heavens (1955) for more details.

trigonometric form of Equation (1) that involves only real values has been derived by Swanepoel (1983).

Since Equation (1) cannot be inverted analytically in order to determine $n(\tilde{\nu})$ and $k(\tilde{\nu})$, an iterative approach must be used. Here, we present a modified approach to the previously published procedures of Hagen et al. (1981) and subsequent studies, with two major changes, described in detail in Section 3: (i) an adaptive step size, and (ii) a more accurate correction step to prevent non-physical results (such as negative n-values that prevent convergence). Moreover, we make one important step further that sets us apart from previous authors: we present and describe the source code itself, with the intent of sharing not only our results, but also the tools that others may use to reproduce those results or to compare them to their own. The source code in Python 3.8 is available for download on Zenodo doi:10.5281/zenodo.3936211 and is free to use and to improve, where the only request is that this work is cited. Note that the Zenodo repository also includes an executable file for the Windows 10 operating system and can be run without a Python installation. Future versions will be updated on both Zenodo and our group's website,[2] from which all of the data presented here also may be downloaded.

Despite the fact that the basic method of Bergren et al. (1978) has been implemented in most laboratory astrophysics studies of IR optical constants, there exist large discrepancies in the results for the same materials (e.g., Ehrenfreund et al. 1997; Baratta & Palumbo 1998). The underlying reasons for these differences may be in the nuances of the experimental techniques of each laboratory, or they may be a result of the details of the algorithm or computer program used to extract the values of n and k from IR spectra. In most cases, it is impossible to determine the true cause, because previous authors either do not provide their original measured spectral data in usable form, or they do not provide their computational code in a format that can be read or modified. Most frequently neither are provided, precluding any truly direct comparisons between laboratory results and preventing any reconciliation of differences. The current work seeks to solve this problem by providing not only our spectral data, but the complete, uncompiled Python computer code that is free to use, implement, and modify without the need for proprietary computer software such as IDL or MATLAB.

Our group has previously studied the IR spectra, band strengths, and, in some cases, the IR optical constants of various molecules relevant to the interstellar medium and to the outer solar system. These include nitriles (Moore et al. 2010), acetylene (Hudson et al. 2014a), ethane and ethylene (Hudson et al. 2014b), amorphous methane (Gerakines & Hudson 2015a), amorphous CO_2 (Gerakines & Hudson 2015b), and nitrous oxide, N_2O (Hudson et al. 2017). All of these studies have included careful measurements of the necessary input parameters for deriving optical constants—namely, the transmission spectrum and visible refractive index. In the following sections, we present in detail our algorithm for determination of IR optical constants, highlighting changes from previous (canonical) approaches in the laboratory astrophysics literature, and present examples to show agreement with some previous results and advantages over some others. Laboratory methods are summarized in Section 2, and our approach and code are detailed in Section 3. Results are presented for some examples, specifically CH_3OH, CO_2, N_2O, and CH_4. Applications to interstellar and planetary ice data from space telescopes are discussed.

[2] http://science.gsfc.nasa.gov/691/cosmicice

2. Laboratory Methods

Ice films in this work were created using techniques described in detail in our recent publications. See, e.g., Hudson et al. (2014b) or Gerakines & Hudson (2015b). In summary, gases were released into a vacuum chamber and allowed to condense onto a cold (lowest $T \sim 10$ K), IR-transparent substrate (KBr or CsI) to produce films with thicknesses up to a few μm. Thicknesses were measured during film growth by monitoring the intensity of a visible-light laser ($\lambda = 670$ nm) passing through the film and substrate with an incidence angle of 0°. Separate films of the same material were studied at a range of different thicknesses (typically, from ~0.25 to 3 μm) to determine optical constants and band strengths. Optical constants for CsI and KBr over the mid-IR wavenumber range were derived from data presented by Li (1976).

Gases to be deposited (CO_2, N_2O, CH_4) were prepared in a manifold connected to the main vacuum chamber through a dosing valve, and any liquids at room temperature and pressure (CH_3OH) were degassed using liquid nitrogen in several freeze-pump-thaw cycles before use.

All values of sample visible refractive index n_{vis} and density ρ used in our optical-constants determinations have been measured directly in our laboratory with the exception of those for CH_4. The procedures have been described in detail previously (e.g., Loeffler et al. 2016). In summary, n_{vis} was determined by combining the information from the interference fringing patterns of two lasers reflected from a sample at different angles of incidence during film growth. Density was determined by monitoring the frequency of a quartz-crystal microbalance during growth of the ice sample. Table 1 lists the values of n_{vis} and ρ used in our calculations.

3. Computational Approach

The algorithm upon which our calculations are based is shown as a flowchart in Figure 1. The primary steps in the procedure are largely identical to those laid out in previous studies in the laboratory astrophysics literature, whose procedures are ultimately derived from that of Bergren et al. (1978). These steps are represented in Figure 1 by the path in black. Significant additional steps have been included to improve upon this standard algorithm, and these modifications are described in the following paragraphs.

As we have attempted to measure the IR optical constants of some of the same films as previous authors, but with higher spectral resolution ($\Delta\tilde{\nu} < 0.5$ cm^{-1}), and for amorphous forms not previously published, we have encountered divergence and non-physical results (e.g., cases that result in $n < 0$). As a result, we have implemented modifications in the iteration procedure that correct for these issues. These changes, described below and shown schematically in Figure 1 as the red, green, and blue paths, yield consistent and stable convergence in cases where the previously published algorithms do not: for films with strong, sharp absorptions where $k > 1$, and for cases of strong, asymmetric absorption profiles —as seen for some amorphous solids—where more commonly used approximations to the k-dependence of their transmittance spectra are not accurate. Each of these scenarios is detailed in this section.

Table 1
Values of Visible Refractive Index and Density Used in These Calculations

Sample	T (K)	n_{vis}	ρ (g cm^{-3})	Source
Amorphous CH_3OH	10	1.296	0.779	Hudson et al. (2020)
Crystalline CH_3OH	120	1.400	1.02	Hudson et al. (2020)
Amorphous CO_2	10	1.27	1.20	Loeffler et al. (2016)
Crystalline CO_2	70	1.40	1.67	Loeffler et al. (2016)
Amorphous N_2O	10	1.317	1.263	Hudson et al. (2017)
Crystalline N_2O	70	1.424	1.591	Hudson et al. (2017)
Amorphous CH_4	10	1.28	0.47	Gerakines & Hudson (2015b), Satorre et al. (2008)
Crystalline CH_4	31	1.32	0.47	Satorre et al. (2008)

3.1. Basic Procedure

As discussed in previous sections, the basic algorithm has been widely used since the 1970s. The algorithm is represented in the flowchart from Figure 1 by the path in black. The initial step (Figure 1, box a) is to process the four required lab-measured input parameters. The first parameter is the film's transmittance spectrum, $T_{lab} = I(\tilde{\nu})/I_0(\tilde{\nu})$, measured in the near- or mid-IR (for the work presented here, we have measured lab spectra for $\tilde{\nu} = 5000$–$500\,cm^{-1}$). The features in the baseline of T_{lab} (overall slope and channel fringes) must be removed before performing the calculations. The second required input parameter is the film's refractive index at an energy higher than that of any strong IR feature found in T_{lab}. In our laboratory, we have measured n_{vis} at 670 nm for every sample studied (details are given by Loeffler et al. 2016). The third required parameter is the sample's thickness h (in cm), typically measured by laser interferometry. The final required input is the set of IR optical constants for the substrate over the same wavenumber range as T_{lab}. For most IR-transparent substrates, the imaginary part is approximately 0 and the real part is approximately constant over the IR range, and this wavenumber-independent behavior often is assumed for simplicity. However, our code allows for values that change with $\tilde{\nu}$, and the optical constants of CsI and KBr used in our results were interpolated from the data compiled by Li (1976).

After the input parameters are given, the initial values of n and k are set as $n(\tilde{\nu}) = n_{vis}$, and $k(\tilde{\nu}) = 0$ for all values of $\tilde{\nu}$ and the initial calculated spectrum is determined using Equation (1) (Figure 1, box b). Next, a correction Δk is determined to improve the k values (Figure 1, box c). We take a general approach, using the Newton–Raphson root-finding method to determine the values of Δk such that $T(n, k + \Delta k)$ is a better approximation to T_{lab}

$$\Delta k = \frac{\ln T_{lab} - \ln T(n,\ k)}{(\partial \ln T/\partial k)|_{n,k}}, \tag{3}$$

where both $T(n,\ k)$ and its partial derivative $\partial \ln T/\partial k$ are evaluated using the current set of n and k.

Most published algorithms determine Δk by way of the absorption coefficients $\alpha(\tilde{\nu})$, which are assumed to change only very little when k is changed to $k + \Delta k$. In this approach,

$$\alpha = 4\pi\tilde{\nu}(k + \Delta k) \approx \left(\frac{1}{h}\right)[-\ln T_{lab} + \ln f(n, k)] \tag{4}$$

(see Hagen et al. 1981, Equation (3)). Here, we use $f(n, k)$ to stand for the second and third terms on the right-hand side of Equation (1)—those that involve the Fresnel coefficients—and is evaluated for the current set of n and k. By examination of Equation (1), $f(n, k) = T(n, k)\, e^{4\pi hk\tilde{\nu}}$. Inserting this expression into Equation (4) and re-arranging terms, we find that

$$\Delta k = \frac{\ln T_{lab} - \ln T(n, k)}{-4\pi h\tilde{\nu}}, \tag{5}$$

which has the same form as Equation (3) but where $\partial \ln T/\partial k \approx -4\pi h\tilde{\nu}$. This approximation for the partial derivative is valid for many IR absorption features, but not for all, and the exceptions can lead to poor (or a complete lack of) convergence in the optical-constants calculation codes published by previous authors. A modification employed in our code allows for the use of more terms in $\partial \ln T/\partial k$ and is described in Section 3.2.

After replacing k with $k + \Delta k$, (Figure 1, box d) the Kramers–Krönig dispersion relation is integrated to obtain the coherent values of n at each wavenumber $\tilde{\nu}_i$

$$n(\tilde{\nu}_i) = n_{vis} + \frac{2}{\pi}\int_{IR} \frac{\tilde{\nu}k(\tilde{\nu})}{\tilde{\nu}^2 - \tilde{\nu}_i^2} d\tilde{\nu}, \tag{6}$$

where Maclaurin's Formula is used to numerically evaluate the integral using the procedure described by Ohta & Ishida (1988), who found this calculation method to be both highly efficient and highly accurate when compared to other approaches. Rocha & Pilling (2014) employ the same integration method, but we have optimized this calculation for speed by utilizing the array operations native to Python's numpy module, evaluating the trapezoidal rule as the scalar product of two 1-D arrays. This method minimizes the use of "for" loops, greatly increasing the speed of the calculation—for example, we have tested our code against the NKABS program of Rocha & Pilling (2014) for the same input spectra and were able to reduce computation times by up to a factor of 100.

After the new n and k values are determined, a new spectrum $T(n, k)$ is calculated using Equation (1), and the channel fringes are removed by dividing by $T(n_{vis},\ 0)$ (Figure 1, box e). The fractional deviation from T_{lab} is determined by $|T(n, k) - T_{lab}|/|T_{lab}|$(Figure 1, box f), and if this deviation at any point falls above the desired maximum constraint (typically 10^{-5}), the k values are again modified by a new correction term Δk (Figure 1, box c) and the iteration cycle continues. Otherwise, the values of n and k are output (Figure 1, box g) and the procedure ends.

We note that some authors have chosen to stop when the average deviation in the spectrum meets a certain goal (e.g., the "mean absolute percent error" used by Rocha & Pilling 2014). However, since the majority of points in a spectrum spanning the mid-IR is in the baseline and not in the absorption features of the sample, the use of the average error can result in very large deviations in the peaks of the absorption features, which

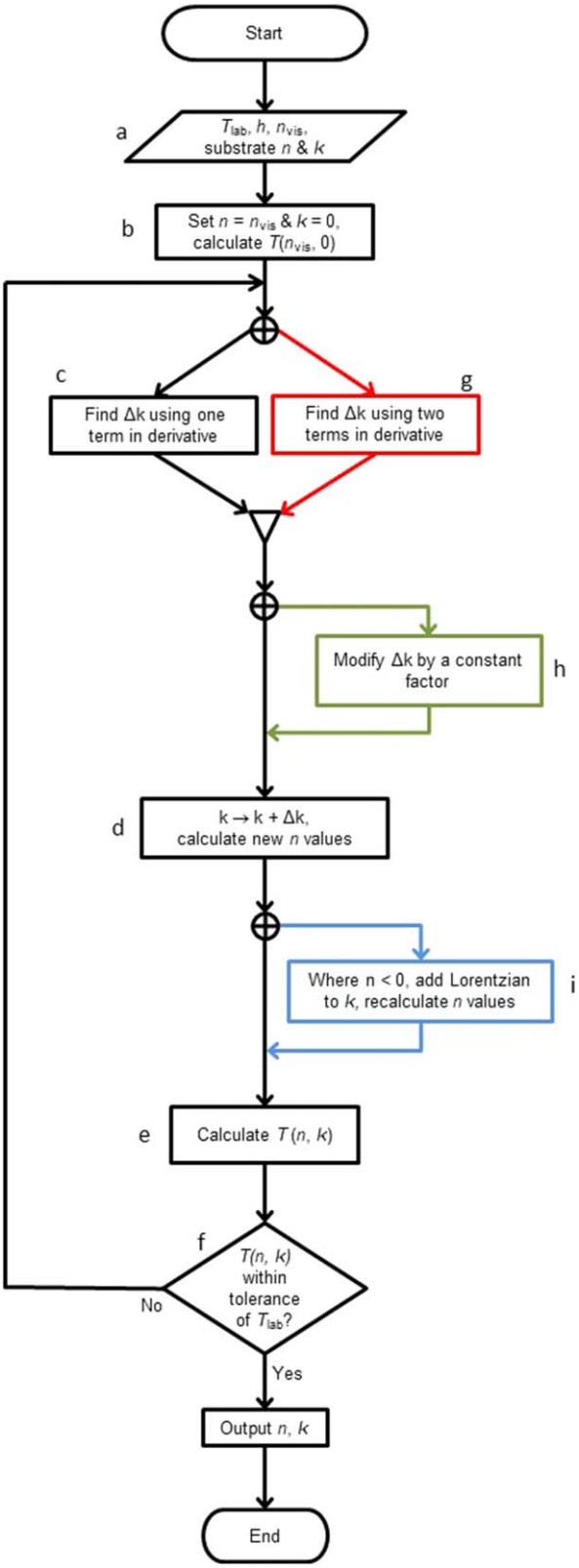

Figure 1. Flowchart of the algorithm used to extract the optical constants n and k from the IR transmission spectrum of an ice film. The path in black represents the algorithm presented by previous authors. The side paths in red, green, and blue represent optional subroutines in our code that overcome conditions that could cause the standard path to fail. The details of each step are described in the text.

are the locations where accuracy is most important to the interpretation of observed spectra. In the examples presented in Section 4, the maximum deviation was typically ∼1000 times higher than the average. Using the stopping criterion of $\sim 10^{-4}$ listed by Rocha & Pilling (2014) as an example, this means that the deviation in the absorption peaks is ∼0.1%. Hence, we use the more stringent requirement that every point in the spectrum must meet the desired goal.

3.2. Modifications to the Basic Procedure

We have made three major modifications to the procedure described in Section 3.1. As far as we are aware, this represents the first time this procedure has been modified in decades. The new steps are represented in Figure 1 by the red, green, and blue paths (boxes g, h, and i, respectively).

The first modification (Figure 1, box g) is to use a higher-order term in the partial derivative $\partial \ln T/\partial k$ in order to find the k correction Δk from Equation (3). To three terms, the partial derivative as derived from Equation (1) is

$$\frac{\partial \ln T}{\partial k} = -4\pi h\tilde{\nu} - \frac{2k}{(1+n)^2 + k^2} - \frac{2(k+k_2)}{(n+n_2)^2 + (k+k_2)^2} + ... \quad (7)$$

As demonstrated above, Hagen et al. (1981) and subsequent authors update k using only the leading term, $-4\pi h\tilde{\nu}$. We have found cases where this approximation is insufficient to converge on a solution (e.g., for amorphous CO_2), but convergence is possible when additional terms are included. In our code, the number of terms can be specified by optional input parameters, but generally the best means to improve convergence behavior in this step is merely to include the second term. A numerical approximation to the derivative (e.g., as determined by finite difference methods) also can be used.

The second modification to the basic algorithm (Figure 1, box h) is to change the magnitude of Δk by multiplying Equation (3) by a constant factor $\beta(<1)$, where $\beta = 0.95$ initially. Applying only a fraction of the full k correction prevents stepping over the solution and then possibly over-correcting, creating an oscillation which either slows or prevents convergence in the iteration process. Optionally, the value of β can be adjusted over the course of the iteration process, depending on the trend in the deviation of $T(n, k)$ from T_{lab} over subsequent iterations. If this option is used, and if the deviation is found to be growing, then β is reduced by ∼5%–10%. If instead the deviation is found to be decreasing, β is increased by ∼1%–5% but not allowed to exceed 0.95. This adjustment has been found to aid in the convergence of cases where IR spectra contain very strong, sharp features, such as for crystalline CO_2. In such spectra, a high-resolution spectrum ($\Delta\tilde{\nu} < 0.5\,cm^{-1}$) can lead to k values much greater than 1 at the locations of absorption peaks and simply applying the approximate correction from Equation (3) without modification can lead to large changes in n that can ultimately cause the algorithm to diverge as it attempts to compensate. Simply starting with a small value of β allows for more applications of Equations (3) and (6) over which n can respond in a more controlled manner to the changes in k and vice versa. This

allows the two parameters to converge more slowly on a solution and avoids numerical errors in the computation.

When nonphysical (negative) values of n are encountered, the third modification (Figure 1, box i) adds a Lorentz oscillator $\Delta k_{\rm L}$ to the correction found in Equation (3) for each negative n value found, where

$$\Delta k_{\rm L}(\tilde{\nu}) = \frac{k_{\rm max}\,(\gamma/2)^2}{(\tilde{\nu} - \tilde{\nu}_0)^2 + (\gamma/2)^2} - \frac{k_{\rm max}\,(\gamma/2)^2}{(\tilde{\nu} + \tilde{\nu}_0)^2 + (\gamma/2)^2} \tag{8}$$

is used to calculate the new term (equation from Ohta & Ishida 1988). The height $k_{\rm max}$, and width γ in Equation (8) are chosen based on the wavenumber spacing of the spectral data and the current values of n (they are also adjustable using optional input parameters). The peak position $\tilde{\nu}_0$ is offset from the location of the negative n value by one width ($+\gamma$). The addition of Δk_L has the largest effect on convergence in the cases of strong absorbers, especially for those measured at high resolution ($\Delta\tilde{\nu} < 0.5\,{\rm cm}^{-1}$), where large variations in n are possible around an absorption peak and the modification of β (as described above) is insufficient to resolve the issue. Adding Lorentzian terms also appears to improve convergence when there are regions of the spectrum over which n and k are simultaneously close to 0. This can be seen in the anomalous dispersion (high-wavenumber) sides of strong, asymmetric absorption features (e.g., for amorphous CO_2 and N_2O). This approach also has been found to make up for inaccurate approximations to $\partial \ln T/\partial k$ used in Equation (3). Examples are discussed in Section 4.

4. Results and Discussion

Here we present some new optical constants and compare them to previously published data. We also demonstrate the reproducibility of previous results using our code and highlight the features discussed in Section 3.

4.1. CH_3OH

For methanol, we compare new results to those in the literature and highlight an issue even for a case where the calculation itself is straightforward. The optical constants of solid methanol have been studied by several previous authors (e.g., Hudgins et al. 1993; Rocha & Pilling 2014; Luna et al. 2018). The IR spectrum of solid CH_3OH is a case that presents no issues with the usual algorithm for calculating n and k, since all derived k values in the mid-IR are less than about 1.1. This is below the value of $n_{\rm vis}$ for CH_3OH, which was measured in our laboratory to be equal to 1.31 ± 0.01 for amorphous CH_3OH at 10 K and 1.44 ± 0.01 for crystalline CH_3OH at 120 K, see Table 1. Figure 2 contains the IR absorbance spectra and optical constants for amorphous and crystalline CH_3OH measured in this study. A comparison of our amorphous CH_3OH results to those of Hudgins et al. (1993) and Rocha & Pilling (2014) is given in Figure 3. The results show significant discrepancies between our three research groups, despite the fact that the algorithm converges quickly (~5 iterations) without the need for adaptive step sizes or other correction procedures. This illustrates the need for the sharing of both laboratory IR spectra and computer codes as we do here, since in those cases the root cause of such differences may be directly studied.

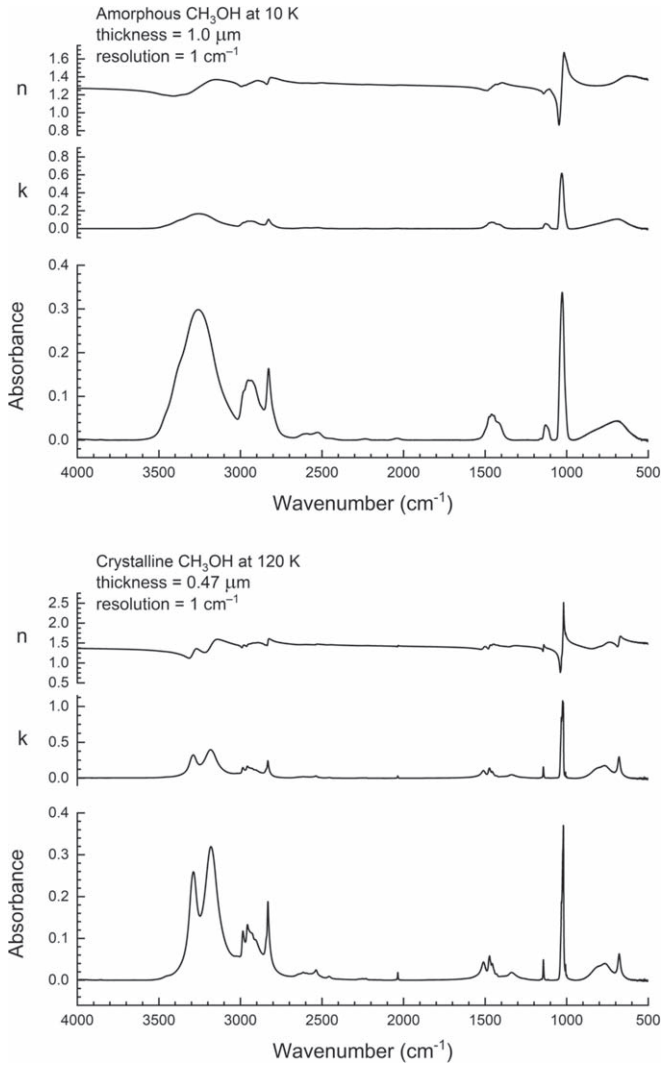

Figure 2. Top panel: measured IR absorbance, and calculated values of n and k for amorphous CH_3OH at 10 K. Absorbance shown for a sample thickness of 1.0 μm, measured with a resolution of 1 cm^{-1} from 4000 to 500 cm^{-1}. Bottom panel: crystalline CH_3OH at 120 K, with a thickness of 0.47 μm, measured with a resolution of 1 cm^{-1} from 4000 to 500 cm^{-1}.

4.2. CO_2

In this section, we highlight a case where the computation of optical constants has been shown to be problematic in the literature but where our algorithm has been applied successfully.

The IR absorbance spectra and calculated IR optical constants for amorphous and crystalline CO_2 are displayed in Figure 4. As has been noted in the literature before, the high-intensity features of CO_2 can result in negative values of n when using the standard method of calculation. This was reported by Poteet et al. (2013) for the case of a crystalline CO_2 ice film they measured at a resolution of 0.1 cm^{-1}. The authors stated that they used a value of $n_{\rm vis} = 1.44$ (from Seiber et al. 1971) to ensure that the calculated n values were positive for all wavenumbers. However, the issue likely was caused not by the value of $n_{\rm vis}$ itself, but by the approximations and procedures used to determine the optical constants that could not take into account the very intense and sharp peaks in k that were

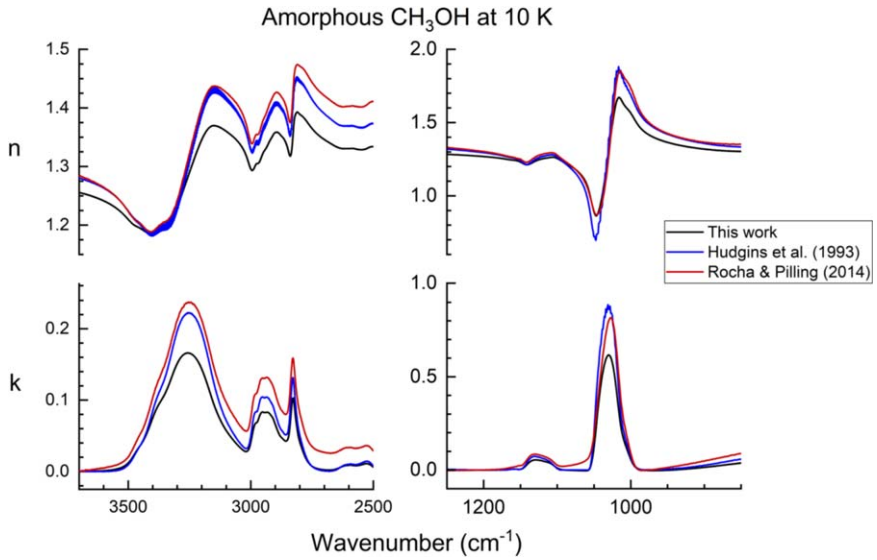

Figure 3. Comparison of our results for amorphous CH_3OH at ∼10 K (black lines) to those of Hudgins et al. (1993; blue) and Rocha & Pilling (2014; red).

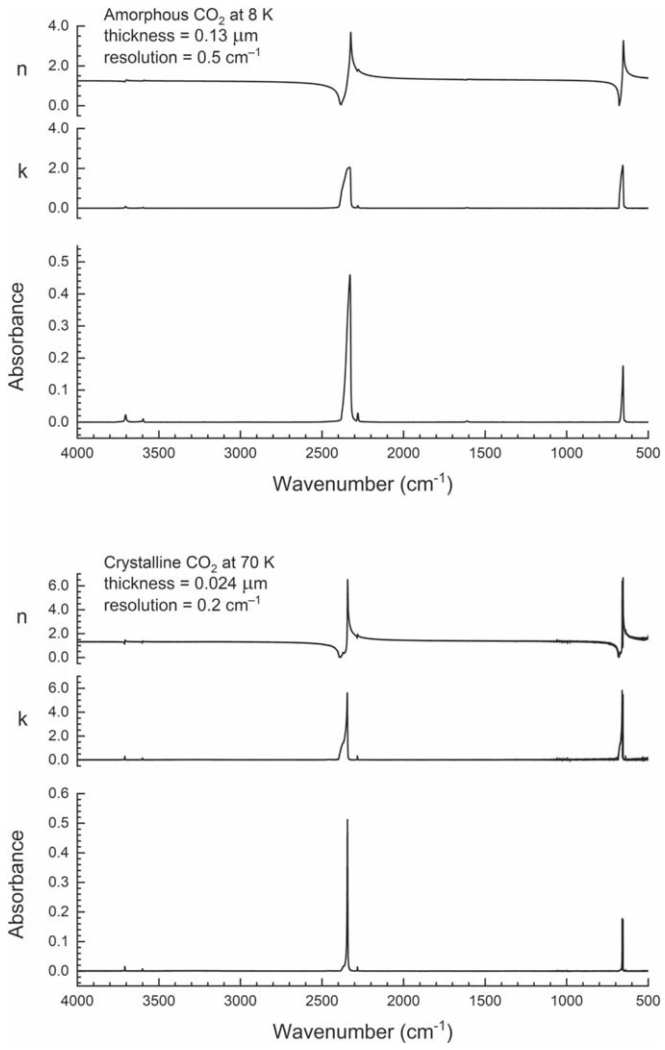

Figure 4. Top panel: measured IR absorbance, and calculated values of n and k for amorphous CO_2 at 8 K. Absorbance shown for a sample thickness of 0.13 μm, measured with a resolution of 0.5 cm^{-1} from 4000 to 500 cm^{-1}. Bottom panel: crystalline CO_2 at 70 K, with a thickness of 0.024 μm, measured with a resolution of 0.2 cm^{-1} from 4000 to 500 cm^{-1}.

encountered. To illustrate this, in Figure 5 intermediate results are shown for two algorithms that start with the same IR spectrum of crystalline CO_2, with the same values of n_{vis} and h as input. In the first case (top half of Figure 5), the first three iterations of the standard algorithm (the black path in Figure 1) are used, as described in Section 3, and this fails after only eight iterations because the algorithm cannot accommodate the negative n values, for which the correction step applies a correspondingly large Δk step, which amplifies the issue and the fractional deviation between $T(n, k)$ and T_{lab} only grows worse with each iteration. The modified algorithm (bottom half of Figure 5) requires a large number of iterations (∼1000) due to the adaptive step size, but ultimately converges on a solution where $T(n, k)$ and T_{lab} agree to 1 part in 10^5. The final result is that shown in the bottom half of Figure 4.

It is perhaps worth noting here that Hudgins et al. (1993) did not report this issue in their extensive set of optical constants calculations. We suspect that this is due to the relatively low resolution of their laboratory IR spectra. Their stated resolution for ice samples such as CO_2 is $\Delta\tilde{\nu} = 1\ cm^{-1}$ in the absorption features and $2\ cm^{-1}$ in the baseline, with only one point every 0.5–1 cm^{-1}. In that case, their spectrum contains under-resolved peaks when considering the crystalline forms of these compounds, since the natural widths of many crystalline ices are below the resolution of their measurements. While this is a widely known, fundamental rule of spectroscopy, it is worth noting here because of the far-reaching ramifications for calculated optical constants and the astrophysical models in which they are implemented. To demonstrate the effect of spectral resolution, in Figure 6 we compare the published CO_2 spectra and optical constants from Hudgins et al. (1993) to our own, which were measured at a resolution of $\Delta\tilde{\nu} = 0.2\ cm^{-1}$. Note that the peaks of the CO_2 features appear more intense at higher resolution, despite the fact that the two samples have similar thicknesses (0.024 versus 0.03 μm). As a check on our method and its consistency with previously reported results, we demonstrate in Figure 6 that our algorithm is able to reproduce the older, under-resolved results using their published IR spectrum and reported input parameters ($n_{vis} = 1.22$ and $h = 0.03\ \mu$m) as the starting point.

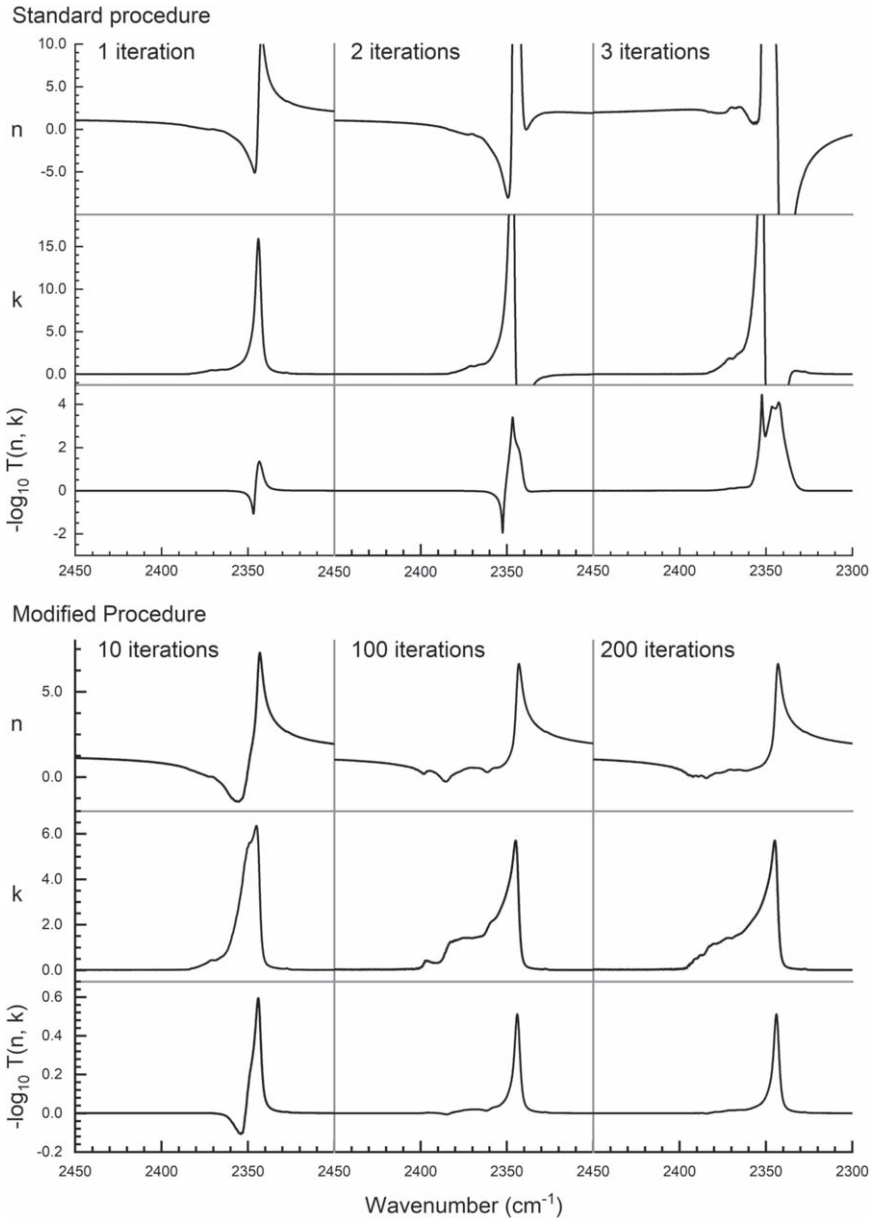

Figure 5. Iteration results using the standard (top panels) and our modified (bottom panels) procedures for determining optical constants, using the case of the IR spectrum of crystalline CO_2 as an example and shown in the range $\tilde{\nu}$ = 2450–2300 cm^{-1}. In the upper set of panels, the standard procedure from the literature was used. In the lower panels, the modified procedure was used, allowing the step size to vary and adding a correction term when negative n values were encountered. Details are described in the text. In the standard case, the code aborted with errors after eight iterations, whereas the modified case proceeded until convergence.

Compared to that of its crystalline phase, the IR spectrum of amorphous CO_2 at 10 K possesses features that are broad and more asymmetric, as documented previously by Gerakines & Hudson (2015b). The observed profiles also have large IR intensities. In addition, amorphous CO_2 has a relatively low value of n_{vis}. These properties in combination lead to simultaneously very small values of n and k around 2375 cm^{-1}, on the high-wavenumber (anomalous dispersion) side of the asymmetric stretching feature. In this case, the denominator of Equation (1) approaches 0, leading to computational difficulties in several steps of the algorithm. Our code addresses these by adding the correction term given in Equation (8) and using only a small fraction of each correction Δk from Equation (3), allowing a gradual convergence in such regions of the spectrum.

4.3. N_2O and CH_4

We have previously studied the physical and optical properties of N_2O, including band strengths, visible refractive indices, and densities for both phases (Hudson et al. 2017). However, optical constants have not yet been reported. The IR spectra of the amorphous and crystalline forms of N_2O have features similar in shape to those of the corresponding phases of CO_2, and the modified procedure was required to successfully converge on a solution for n and k. Here, in Figure 7, we present the first set of mid-IR optical constants for amorphous N_2O at 10 K using n_{vis} = 1.32 and for a sample thickness of 0.25 μm and also for crystalline N_2O at 70 K using n_{vis} = 1.42 and the spectrum of a sample with a thickness of 0.24 μm.

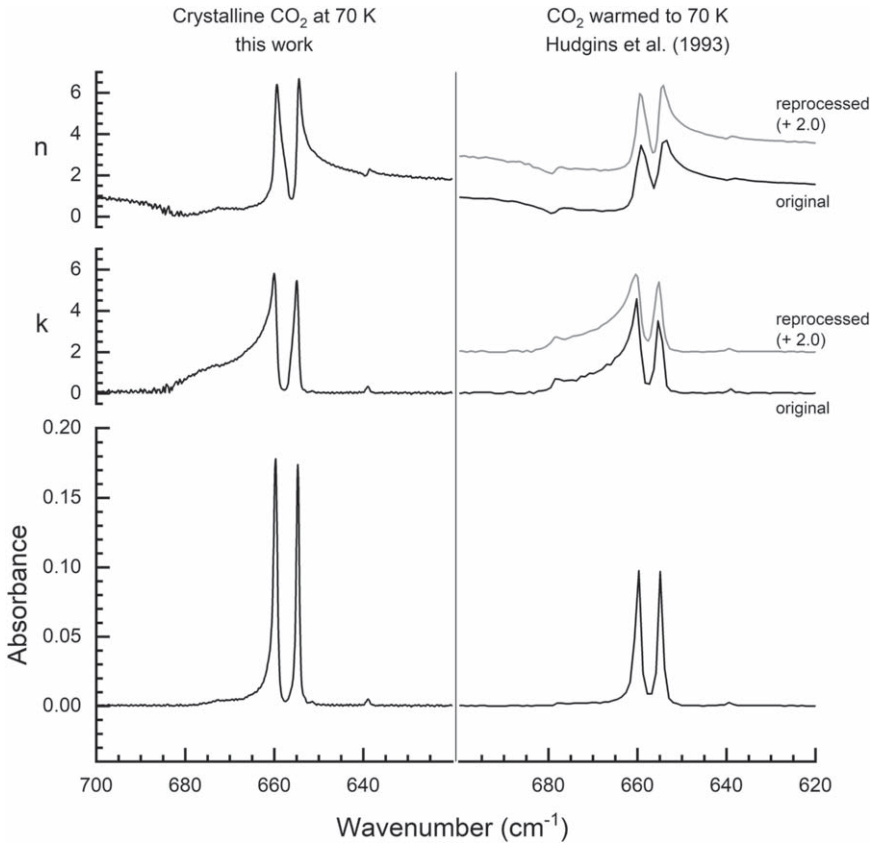

Figure 6. IR spectra and optical constants of crystalline CO_2 from 700 to 620 cm^{-1} as measured in this work (left panels), in comparison to those published by Hudgins et al. (1993) for a sample of similar thickness but measured at lower spectral resolution (right panels). Left panels: data from Figure 4 (crystalline CO_2 sample with a thickness of 0.024 μm, $n_{vis} = 1.40$, and measured with a resolution of 0.2 cm^{-1}). Right panels, black lines: original data from Hudgins et al. (1993) for a CO_2 sample deposited at 10 K with a thickness of 0.03 μm, $n_{vis} = 1.22$, heated to 70 K, and measured with a resolution between 1 and 2 cm^{-1}. Right panels, gray lines: optical constants calculated with our modified algorithm to demonstrate repeatability. An offset of 2.0 has been added to the reprocessed optical constants for clarity.

Table 2
Absolute Absorption Coefficients and Absolute Band Strengths for Selected IR Features

Sample	Peak position (cm^{-1})	Absolute absorption coefficient, α(cm^{-1})	Integration range (cm^{-1})	Absolute band strength, A (cm molecule^{-1})
Amorphous CH_3OH	2827.9	3657.4	2868–2757	5.31×10^{-18}
	1030.3	8014.7	1066–967	1.68×10^{-17}
Crystalline CH_3OH	2832.0	8711.9	2874–2792	6.64×10^{-18}
	1024.6	13891	1062–992	1.27×10^{-17}
Amorphous CO_2	2331.0	60270	2441–2289	1.81×10^{-16}
	656.4	17741	692–631	2.08×10^{-17}
Crystalline CO_2	2344.9	165490	2410–2319	1.30×10^{-16}
	660.1, 655.0	48160, 44967	689–647	1.86×10^{-17}
Amorphous N_2O	2225.1	38168	2266–2200	6.23×10^{-17}
	1285.2	11762	1311–1262	1.19×10^{-17}
	588.7	4079.1	601–573	1.86×10^{-18}
Crystalline N_2O	2237.2	108210	2261–2232	5.74×10^{-17}
	1293.3	42841	1304–1280	9.58×10^{-18}
	589.0	18918	595–583	1.67×10^{-18}
Amorphous CH_4	3010.5	23784	3160–2930	1.41×10^{-17}
	1298.3	18598	1345–1255	1.03×10^{-17}
Crystalline CH_4	3011.4	11498	3133–2946	1.36×10^{-17}
	1300.2	18418	1402–1222	9.88×10^{-18}

Methane has also been previously studied by us (Gerakines & Hudson 2015a), where we reported the first IR spectrum and set of IR intensities of the amorphous form at 10 K. Optical constants were also presented for amorphous CH_4 at 10 K. Due to the relatively low values of k in the absorption peaks, as compared to those of CO_2 or N_2O, no modified procedures were necessary to converge on a solution. Here, we present the first full set of mid-IR results for both the amorphous form of

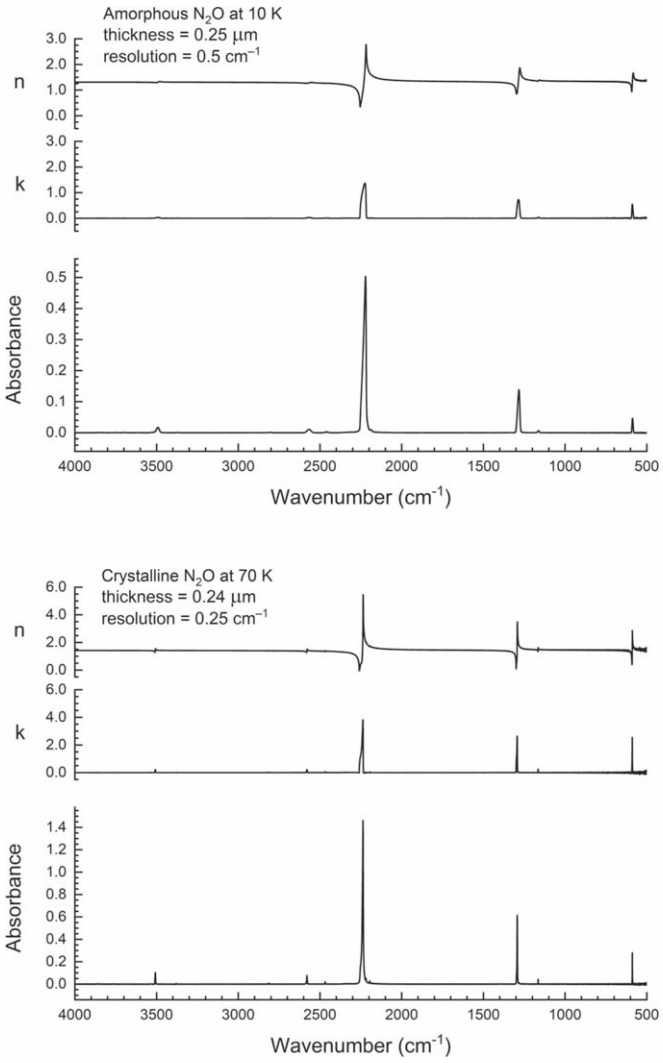

Figure 7. Top panel: measured IR absorbance, and calculated values of n and k for amorphous N_2O at 10 K. Absorbance shown is for a sample thickness of 0.25 μm, measured with a resolution of 0.5 cm^{-1} from 4000 to 500 cm^{-1}. Bottom panel: crystalline N_2O at 70 K, with a thickness of 0.24 μm, measured with a resolution of 0.25 cm^{-1} from 4000 to 500 cm^{-1}.

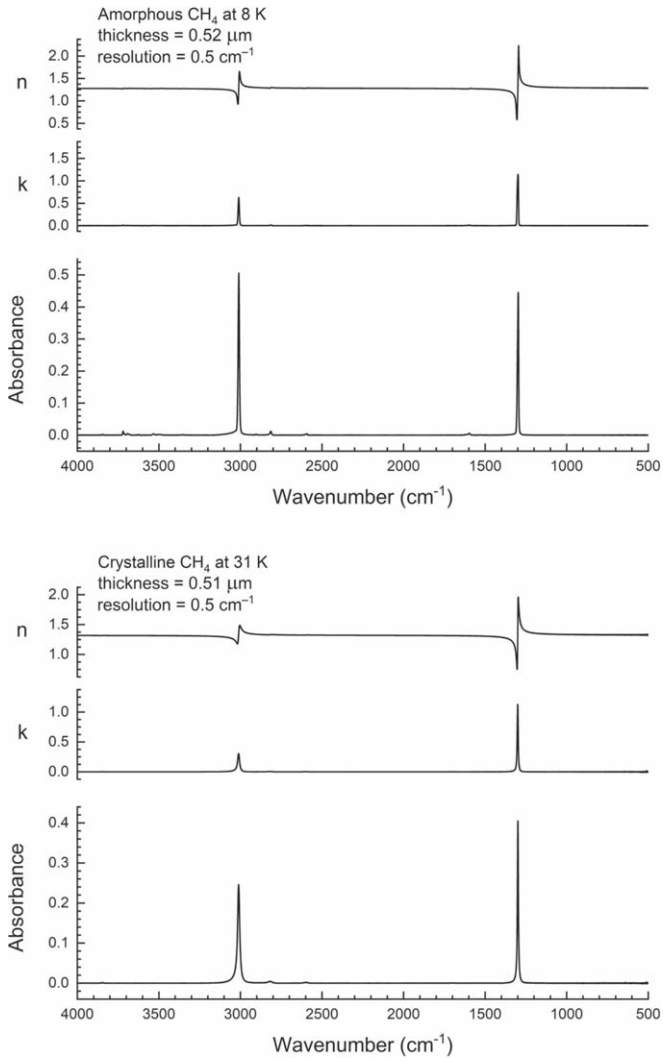

Figure 8. Top panel: measured IR absorbance, and calculated values of n and k for amorphous CH_4 at 8 K. Absorbance shown is for a sample thickness of 0.52 μm, measured with a resolution of 0.5 cm^{-1} from 4000 to 500 cm^{-1}. Bottom panel: crystalline CH_4 at 31 K, with a thickness of 0.51 μm, measured with a resolution of 0.5 cm^{-1} from 4000 to 500 cm^{-1}.

CH_4 at 10 K and the high-temperature crystalline form at 31 K in Figure 8. Values of n_{vis} used were 1.28 and 1.32, respectively (see Table 1).

4.4. Absorption Coefficients and Band Strengths

Optical constants may be used to derive other useful quantities for the analysis of astronomical spectra. Specifically, the IR absorption coefficient $\alpha(\tilde{\nu})$ (in cm^{-1}) and band strength A (in cm molecule^{-1}) of a spectral feature can be found, where

$$\alpha(\tilde{\nu}) = 4\pi\tilde{\nu}k(\tilde{\nu}), \tag{9}$$

and

$$A = \frac{1}{\rho_N}\int_{\text{band}} \alpha(\tilde{\nu})d\tilde{\nu}, \tag{10}$$

where ρ_N is the number density of the absorbers (in molecules cm^{-3}) and the integration in Equation (10) is taken over the range of the absorption band of interest. The value of A can then be used to determine the column density of a molecule whose absorption feature appears in the IR spectrum of an interstellar cloud. When determined using the optical constants, α is known as the absolute absorption coefficient and A is known as the absolute band strength. This is to distinguish them from the corresponding apparent quantities that are obtained from a measured IR spectrum. See discussions by Maeda & Schatz (1961) and Hudson et al. (2014a, 2014b) for more details about this distinction. Values of $\alpha(\tilde{\nu})$ and A for selected features in the spectra shown in Figures 2, 4, 7, and 8 are given in Table 2. For previous studies of these properties, we refer the reader to a comprehensive bibliographic review of the literature by Bouilloud et al. (2015).

5. Summary and Conclusions

Here, we present our Python code, written to be shared with the general community. This code was developed with modifications to the standard algorithm, avoiding numerical issues that otherwise prevent convergence on a coherent set of results in n and k. It also is our goal in this work to pull back

the curtain and provide not only the final numbers but the means by which they can be duplicated or checked against those of other laboratories.

Most laboratory studies of optical constants in the literature are presented with a brief summary of the steps in their numerical algorithm, but very few, if any, have included their code. This creates difficulties for readers that would wish to duplicate the presented results or to process their own laboratory data in exactly the same manner. Several such reports exist, and while most employ the same basic algorithm, their final results often have significant differences that cannot be directly explained or studied using the information given.

For example, Rocha & Pilling (2014) present a large set of optical constants results and provide their compiled program, which is unreadable without the use of special Python modules. While their algorithm largely follows that of Hudgins et al. (1993), it does not appear to have any calculation step that corrects for channel fringes in the baseline of the calculated spectra. Moreover, their program uses the deviation of the calculated spectrum from the input lab spectrum averaged over the entire spectrum ("mean average percent error") as the stopping criterion, as discussed earlier.

The properties of a transmission spectrum are largely moderated by the properties of $k(\tilde{\nu})$, where the Beer–Lambert Law dominates the absorption trend with thickness (i.e., $\ln T \approx -\alpha h$). Thus, the standard approximation to the k correction in Equation (5) is a reasonable one in many cases. However, as we have shown for CO_2, there are cases where the IR intensities are high but the values of $n_{\rm vis}$ are low, leading to k corrections that ultimately lead to numerical instabilities in computer programs to determine n and k from mid-IR spectra. In such spectral regions, as in the anomalous dispersion of strong absorbers, the inclusion of an n-correction step (based on the partial derivative $\partial \ln T/\partial n$) in the algorithm may provide an improved convergence behavior. A method of extracting optical constants from reflectance data using simultaneous corrections in both n and k was presented by Leveque & Villachonrenard (1990), but to our knowledge this procedure has yet to be developed for transmittance. Future work could address this.

On a final note, we also present absolute absorption coefficients and band strengths derived from these calculations of optical constants. Interstellar abundances are as mathematically dependent on the accuracy of the value of band strengths as they are on the accuracy of the telescopic data from which they are derived. Therefore, laboratory efforts to produce high-quality physical and optical parameters (such as the ones presented here) are paramount to understanding the chemistry of interstellar environments.

The authors would like to thank W. J. Moore and M. H. Moore for advice and suggestions in the early stages of this study. This work was supported by the NASA APRA and PDART programs, as well as the NASA-GSFC FLaRe ISFM program.

ORCID iDs

Perry A. Gerakines https://orcid.org/0000-0002-9667-5904
Reggie L. Hudson https://orcid.org/0000-0003-0519-9429

References

Baratta, G. A., & Palumbo, M. E. 1998, JOSAA, 15, 3076
Bergren, M. S., Schuh, D., Sceats, M. G., & Rice, S. A. 1978, JChPh, 69, 3477
Bouilloud, M., Fray, N., Benilan, Y., et al. 2015, MNRAS, 451, 2145
Ehrenfreund, P., Boogert, A. C. A., Gerakines, P. A., Tielens, A. G. G. M., & van Dishoeck, E. F. 1997, A&A, 328, 649
Gerakines, P. A., & Hudson, R. L. 2015a, ApJL, 805, L20
Gerakines, P. A., & Hudson, R. L. 2015b, ApJL, 808, L40
Hagen, W., Tielens, A. G. G. M., & Greenberg, J. M. 1981, CP, 56, 367
Heavens, O. S. 1955, Optical Properties of Thin Solid Films (London: Butterworths Scientific Publications)
Hudgins, D. M., Sandford, S. A., Allamandola, L. J., & Tielens, A. G. G. M. 1993, ApJS, 86, 713
Hudson, R. L., Ferrante, R. F., & Moore, M. H. 2014a, Icar, 228, 276
Hudson, R. L., Gerakines, P. A., & Moore, M. H. 2014b, Icar, 243, 148
Hudson, R. L., Loeffler, M. J., Ferrante, R. F., Gerakines, P. A., & Coleman, F. M. 2020, ApJ, 891, 22
Hudson, R. L., Loeffler, M. J., & Gerakines, P. A. 2017, JChPh, 146, 024304
Leveque, G., & Villachonrenard, Y. 1990, ApOpt, 29, 3207
Li, H. H. 1976, JPCRD, 5, 329
Loeffler, M. J., Moore, M. H., & Gerakines, P. A. 2016, ApJ, 827, 98
Luna, R., Molpeceres, G., Ortigoso, J., et al. 2018, A&A, 617, A116
Maeda, S., & Schatz, P. N. 1961, JChPh, 35, 1617
Moore, M. H., Ferrante, R. F., Moore, W. J., & Hudson, R. 2010, ApJS, 191, 96
Muller, R. H. 1969, SurSc, 16, 14
Ohta, K., & Ishida, H. 1988, ApSpe, 42, 952
Poteet, C. A., Pontoppidan, K. M., Megeath, S. T., et al. 2013, ApJ, 766, 117
Rocha, W. R. M., & Pilling, S. 2014, SpAcA, 123, 436
Satorre, M. A., Domingo, M., Millan, C., et al. 2008, P&SS, 56, 1748
Seiber, B. A., Smith, A. M., Wood, B. E., & Müller, P. R. 1971, ApOpt, 10, 2086
Swanepoel, R. 1983, JPhE, 16, 1214